

pubs.acs.org/cm Article

Predicting Thermal Quenching in Inorganic Phosphors

Mahdi Amachraa,[§] Zhenbin Wang,[§] Chi Chen, Shruti Hariyani, Hanmei Tang, Jakoah Brgoch, and Shyue Ping Ong*



Cite This: Chem. Mater. 2020, 32, 6256-6265



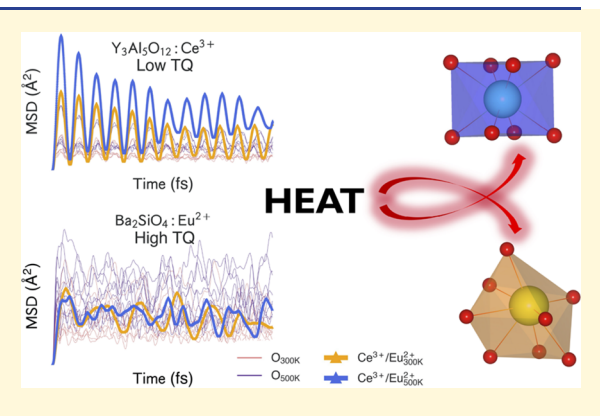
ACCESS

Metrics & More

Article Recommendations

Supporting Information

ABSTRACT: Phosphor-converted light emitting diodes (LEDs) are a highly efficient form of solid-state lighting. A key performance metric of a phosphor is its thermal quenching (TQ), which is the percentage loss of emission at elevated temperatures during operation. In this work, we unify the two prevailing theories—the crossover and thermal ionization mechanisms—into a single predictive model for TQ. Using *ab initio* molecular dynamics (AIMD) simulations, we demonstrate for the first time that TQ under the crossover mechanism is related to the local environment stability of the activator. Further, by accounting for the effect of the crystal field on the thermal ionization barrier, we show that a unified model can predict the experimental TQ in 29 known phosphors to within a root-mean-square error of ~3.1–7.6%. Finally, we propose an efficient topological approach to rapidly screen vast chemical spaces for the discovery of novel, thermally robust phosphors.



■ INTRODUCTION

General lighting accounts for approximately 15% of global energy consumption and 5% of CO₂ emissions. Modern white lighting based on phosphor-converted light-emitting diodes (pc-LEDs) is $\sim 10 \times$ more efficient than traditional lighting and therefore offers a huge opportunity to achieve substantial energy savings and CO₂ reduction. A critical component in pc-LEDs is the rare-earth substituted inorganic phosphor, which down-converts the near-ultraviolet or blue LED emission to longer wavelengths. The phosphors currently employed in these bulbs comprise an inorganic host material, such as an oxide or nitride, activated with a rare-earth ion that is typically Ce³⁺ or Eu²⁺. The prototypical phosphor used in a majority of devices is yttrium aluminum garnet, Y3Al5O12, activated with Ce³⁺ (YAG:Ce³⁺) to produce a bright yellow emission. Exciting this phosphor when it is coated on top of a blue LED chip produces a broad emission across the visible spectrum light, appearing as white light.

Developing phosphors with high quantum efficiency and excellent thermal stability is a long-standing quest in solid-state lighting. Emission loss with increasing temperature (also known as thermal quenching or TQ) is of particular importance in next-generation lighting, where high-power and laser-based LEDs are becoming more common. In combination with smaller device packaging, the heat generated in these devices can negatively influence the optical output, in particular from the phosphor.² The TQ of a phosphor is experimentally determined by taking the ratio between the integrated light intensity emitted at the operating temperature (~423–473 K) and the integrated intensity of light emitted at

room temperature. Commercial phosphors, such as YAG: Ce^{3+} , have a TQ of less than 10%, meaning a majority of the room temperature emission intensity is maintained at high temperature, whereas other phosphors can be entirely thermally quenched (TQ = 100%) at high temperature. It is therefore unsurprising that extensive efforts have been devoted to the investigation of the TQ mechanism in phosphors.³⁻⁶

Two dominant theories have been proposed to explain the TQ behavior in Ce3+- and Eu2+-activated phosphors. In the 1960s, Blasse et al. proposed that TQ is the result of the nonradiative relaxation of electrons from the excited state to the ground state.^{7,8} This crossover mechanism is represented schematically using the configurational coordinate diagram in Figure 1, where the energy difference between the relaxed excited state and the crossover point determines the activation barrier E_a^{co} for this process. This theory is one of the reasons why there is a search for structurally rigid phosphor hosts. The fundamental assumption is that a more rigid host prevents access to soft phonon modes, reducing the probability of nonradiative relaxation from the excited configuration to the ground state configuration. However, subsequent experiments have found many violations of this relationship. For example, the Ca₇Mg(SiO₄)₄:Eu²⁺, CaMgSi₂O₆:Eu²⁺, and

Received: May 27, 2020 Revised: July 1, 2020 Published: July 6, 2020





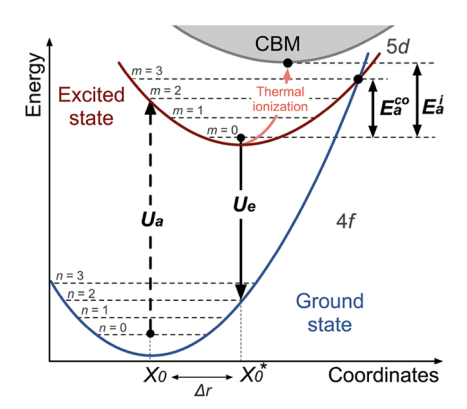


Figure 1. Configurational coordinate diagram for the activator in a phosphor. Excitation is allowed from the vibrational level n=0 of the ground state to the excited state and results in the absorption energy U_a . The relaxation of the system from the vibrational level m=0 to the ground state results in the emission energy U_e . The displacement $\Delta r = X_0^* - X_0$ is the polyhedron average bond length difference between the excited and the ground states of the activator. In the crossover model, thermal quenching results from the nonradiative relaxation of an excited electron to the ground state when the temperature is high enough to overcome the activation energy E_a^{co} . In the Dorenbos thermal ionization model, thermal quenching results from the promotion of excited electrons to the conduction band minimum if the temperature is high enough to overcome the activation energy E_a^i .

 $Sr_6M_2Al_4O_{15}$: Eu^{2+} (M = Y, Lu, Sc) phosphors all suffer from TQ despite their seemingly rigid crystal structures, as estimated from their comparatively high Debye temperatures. ^{9,10} The second theory, attributed to Dorenbos, posits that TQ is due to the thermal excitation of the excited 5d electron of Ce^{3+}/Eu^{2+} to the conduction band of the host; ⁶ the activation barrier of this thermal ionization process (E_a^i in Figure 1) determines the TQ of a phosphor. Other TQ

pathways have been suggested as well; e.g., the temperature dependence of the conduction band minimum is expected to lower E_a^i and induces TQ_a^3 although the two competing mechanisms (crossover mechanism and thermal ionization process) dominate in the loss of luminescence as a function of temperature in Ce³⁺/Eu²⁺-activated phosphors. In this work, we develop a unified theory of TQ in phosphors by considering the competition between the two dominant TQ mechanisms. It should be noted that all other forms of quenching, thermal or otherwise, are not considered in this model. The focus of this work is specifically on TQ in Ce³⁺ and Eu2+-activated oxide phosphors, which are the most common rare-earth ions employed in phosphors and operate on the highly efficient $4f''5d^0 \rightarrow 4f''^{-1}5d^1$ transition. Using ab initio molecular dynamics simulations (AIMD), we establish that the local environment stability around the rare-earth ion as a function of temperature is a robust, transferable descriptor for TQ under the crossover mechanism when the host band gap is sufficiently large. If the host band gap is small, however, the thermal ionization mechanism competes with the crossover mechanism. We, therefore, develop a model accounting for both quenching mechanisms to predict the TQ of known phosphors. A total of 29 oxide phosphors with experimentally measured TQ values were selected to construct the models. Information on these phosphors is summarized in Table S1. Our results show that the combination of AIMD simulations and band gap (E_{σ}) calculations provides a clear relationship between a series of computed descriptors and a phosphor's TQ behavior. Furthermore, we propose a novel topological descriptor based on the Voronoi analysis that can be used to rapidly screen for low TQ phosphors without expensive AIMD simulations, thereby allowing the discovery of new thermally robust inorganic phosphors.

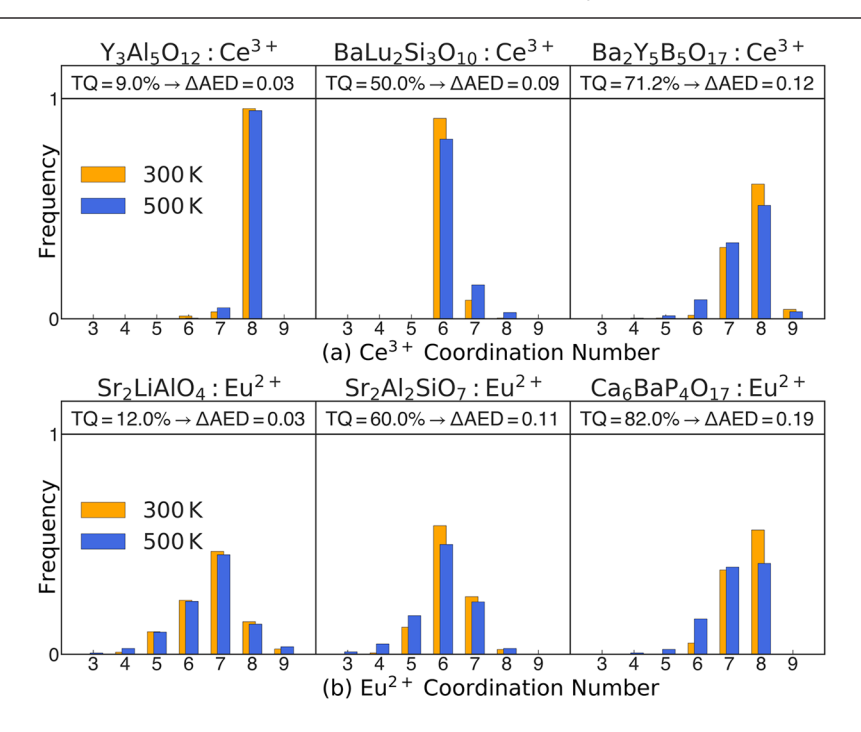


Figure 2. Activator environment distribution (AED). The computed AED of (a) Ce^{3+} and (b) Eu^{2+} at 300 and 500 K in three hosts with distinct TQ behaviors. The experimental TQ values were obtained from refs 13-18.

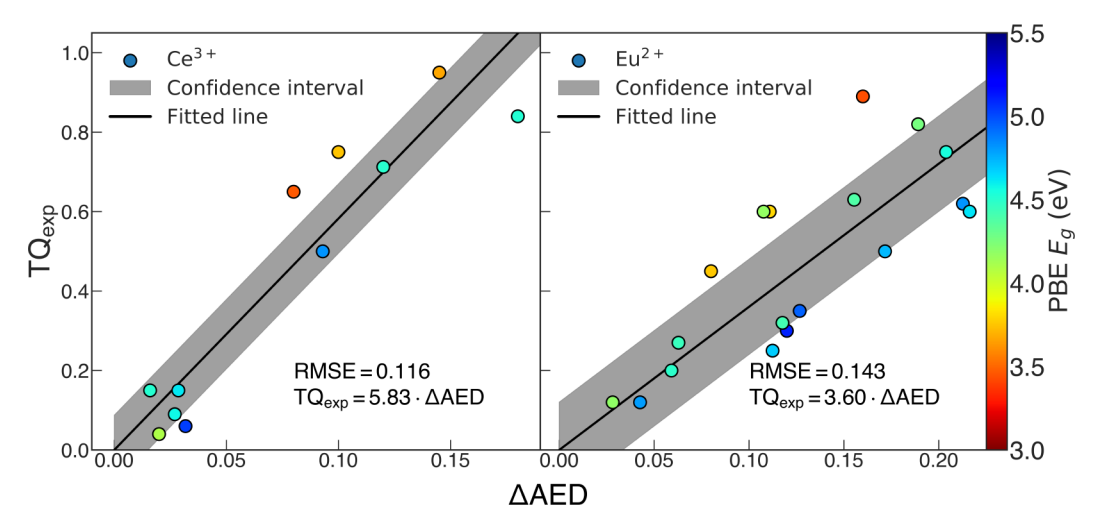


Figure 3. Local environment rigidity. Plot of the experimental thermal quenching (TQ_{exp}) against the change in the activator environment distribution (ΔAED) for Ce^{3+} (left) and Eu^{2+} (right) activated phosphors. The marker colors are based on their calculated band gap using the Perdew-Burke-Ernzerhof (PBE) functional (see color bar). The root-mean-square error (RMSE for each model is defined as the square root of the average squared difference between the computed ΔAED and the experimental TQ (TQ_{exp}) , i.e., $RMSE = \sqrt{\frac{1}{N}\sum_{i=1}^{N} (TQ_{exp}^{i} - K \cdot \Delta AED^{i})^{2}}$.

■ RESULTS AND DISCUSSION

Relationship between Thermal Quenching and Local **Environment Rigidity.** AIMD simulations were performed on the 29 phosphors at room temperature (300 K) as well as 500 K to represent an upper-temperature limit experienced by the phosphor during lamp operation. 11 An activator environment distribution (AED) at both temperatures was constructed for each phosphor from the AIMD trajectories. The AED is derived by determining the number of simulation time steps at which the activator has a particular coordination number (CN) using the algorithm developed by Waroquiers et al., ¹² normalized across the total number of time steps. Figure 2 presents the AED for three Ce³⁺- and three Eu²⁺-activated phosphors with high (>80%), intermediate (40-60%), and low (<20%) TQ. Similar plots for the remaining 23 phosphors are provided in Figures S3 and S4. Comparing the AEDs between 300 and 500 K shows that thermally robust (small TQ) phosphors generally exhibit minimal change in the AED as a function of temperature whereas thermally quenched (high TQ) phosphors show substantial shifts in the AED with temperature. For example, the Ce^{3+} in YAG: Ce^{3+} (TQ = 9%) is primarily 8-fold coordinated with oxygen, and its CN remains stable at 500 K. In contrast, the Ce^{3+} in $Ba_2Y_5B_5O_{17}$: Ce^{3+} (TQ = 71%) has a CN distribution of 7-8 at 300 K and exhibits an obvious shift to lower CNs, including 7-fold and 6-fold coordination environments, at 500 K. The same trend is observed for Eu²⁺-activated phosphors in Figure 2b.

To quantify the shift in the AED from 300 to 500 K, we define ΔAED as the Euclidean distance between AEDs at 300 and 500 K in eq 1,

$$\Delta AED = \sqrt{\sum_{x=2}^{12} \left(\omega_{\text{CN}=x}^{300\text{K}} - \omega_{\text{CN}=x}^{500\text{K}}\right)^2}$$
 (1)

where $\omega_{\text{CN}=x}^{300\text{K}}$ and $\omega_{\text{CN}=x}^{500\text{K}}$ are the normalized CN frequencies at 300 and 500 K, respectively, and the CN ranges from 2 to 12. Figure 3 shows the experimentally measured TQ (TQ_{exp}) plotted against the computed ΔAED for Ce³⁺ and Eu²⁺-activated phosphors. We find there is an approximately linear positive correlation between TQ and ΔAED for both Ce³⁺-

and Eu²⁺-activated oxide phosphors. A least-squares fitting for the one-parameter expression $TQ = K \cdot \Delta AED$, where K is a constant, yields R² values of 0.89 and 0.62 for Ce³⁺- and Eu²⁺activated phosphors, respectively, with reasonable root-meansquare errors (RMSEs) of 11.6% and 14.3%, respectively. In contrast, the DFT-calculated Debye temperature (Θ_D) yields a weaker correlation against TQ_{exp} (see Figure S5) with R^2 values of 0.14 and 0.12 for Ce³⁺- and Eu²⁺-activated phosphors, respectively, and corresponding root-mean-square errors (RMSEs) of 32% and 26%, respectively. Although, there is some correlation between \triangle AED and host structural rigidity. as suggested by the high Debye temperatures, the coordinated local displacements within a crystal environment are more directly related to the low ΔAED , making it more reliable compared to a global descriptor like structural rigidity. These observations support our hypothesis that ΔAED is an effective descriptor to probe the depth of the potential energy surface (PES) in the crossover model, where a higher Δ AED implies a shallower PES in the ground and excited states, which results in a lower E_a^{co} and higher TQ.

Accounting of Thermal Ionization. A closer examination of Figure 3 further reveals that phosphors with large host band gaps (E_g) lie below the regression line, and those with small E_g lie above the line. This observation suggests that E_g , which is related to TQ under the Dorenbos single-barrier quenching model, also plays a critical role for some materials. Figure 4 shows a schematic of the energy levels of a Ce^{3+}/Eu^{2+} activator in a host. It can be seen that the Dorenbos thermal ionization barrier is given by

$$E_a^i(A^{x+}, H) = E_g - \left[E(A^{x+}, \text{ free}) - \varepsilon_c(A^{x+}, H) - \frac{\varepsilon_{cfs}(A^{x+}, H)}{r(H)} + \varepsilon_s(A^{x+}, \text{ free}) \right] - E(4f^n - VBM)$$
(2)

where E_g is the band gap of the host, $E(A^{x+}, \text{free})$ is the fixed centroid position for the free A^{x+} ion $(E(Ce^{3+}, \text{free}) = 6.118 \text{ eV})$ and $E(Eu^{2+}, \text{free}) = 4.216 \text{ eV})$, 19 $\varepsilon_c(A^{x+}, H)$ is the centroid

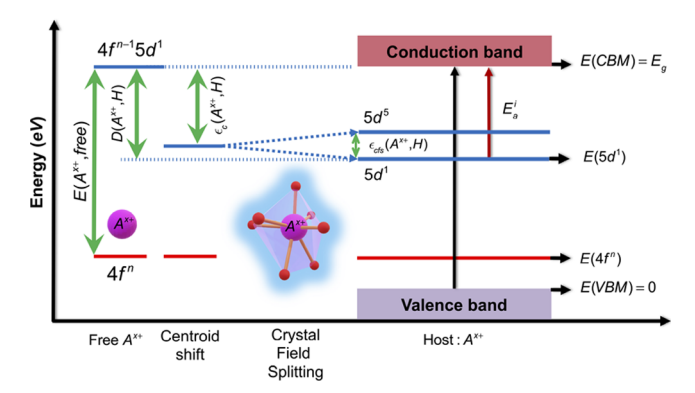


Figure 4. Energy level diagram for Ce^{3+}/Eu^{2+} activators (denoted by A^{x+} in a host material denoted by A^{x+}). The $\varepsilon_c(A^{x+}, A^{x+})$, $\varepsilon_{cfs}(A^{x+}, A^{x+})$, $E_{cfs}(A^{x+}, A^{x+})$, and $E(A^{x+}, A^{x+})$ refer to the centroid shift, crystal-field splitting, the redshift of the activators A^{x+} for A^{x+} levels in a host A^{x+} respectively, and the energy of the first A^{x+} for A^{x+} d. The VBM and CBM indicate the valence band maximum and the conduction band minimum, respectively. Note that the energy of the VBM is the energy referential and is set to A^{x+} even A^{x+} of A^{x+} refers to the lowest excited A^{x+} energy state with an electron relaxed from the higher energy levels.

shift for A^{x+} in the host H, $\varepsilon_{cfs}(A^{x+},\ H)$ is the crystal-field splitting experienced in the host H, r(H) expresses the ratio between the crystal-field splitting and the crystal-field shift (typical values range between 1.7 and 2.4 and is geometry dependent), $\varepsilon_s(A^{x+}$, free) is the energy difference between the centroid position and the lowest 5d level of the free A^{x+} ion and is also a constant, and $E(4f^n-VBM)$ is the energy difference between the $4f^n$ of A^{x+} and the valence band maximum (VBM) of the host H. The binding energy $E(4f^n)$ for Ce³⁺ has been found to be relatively constant for garnets and perovskites and will be assumed constant for the 11 Ce3+doped hosts considered in the study, while $E(4f^n)$ for Eu^{2+} has an energy fluctuation of ~0.38 eV in oxides depending on the host H^{20} r(H) is assumed to be 5/2 for 6-coordinated geometries and 5/3 for 8-coordinated geometries.²¹ For brevity, we will drop the explicit functional dependence of the variables henceforth.

Equation 2 can be modified in terms of DFT computed quantities as follows:

$$E_a^i = A E_g^{DFT} + B \varepsilon_c^{DFT} + \frac{1}{r} \left(C \frac{\Theta_0^2}{l_{avg}^3} + D \frac{\Theta_0^4}{l_{avg}^5} \right) + E$$
 (3)

where ε_c^{DFT} can be evaluated using the ligand polarization model, $^{20}\varepsilon_{cfs}$ is expressed expressed as the sum of both secondand fourth-rank crystal-field parameters Θ_0^2 and Θ_0^4 as $\varepsilon_{cfs} = C \frac{\Theta_0^2}{l_{avg}^3} + D \frac{\Theta_0^4}{l_{avg}^5}$, and l_{avg} is an average polyhedron bond length around the activator. Detailed derivations are provided in the Supporting Information. Here, A, B, C, D, and E are fitted constants, where A accounts for the well-known underestimation of E_g by the PBE functional, 22 while B accounts for systematic errors in the estimation of the centroid shift from the DFT lattice parameters (refer to eq S4 in the Supporting Information). Finally, C and D account for the mutual importance of the second- and fourth-rank crystal-field parameters, as well as the refactoring of the computed ε_{cfs} energies with respect to the computed E_g^{DFT} and ε_c^{DFT} .

Considering the crossover model and the thermal ionization model for quenching are two independent sources of TQ, both are likely occurring simultaneously in some phosphor systems. Therefore, we combine ΔAED with the Dorenbos expression for TQ^6 under the thermal ionization model (detailed derivations are provided in the Supporting Information) to arrive at the following formula of TQ_{pred} :

$$TQ = 1 - (1 - K \cdot \Delta AED) \frac{1 + \Gamma \cdot \frac{-E_a^i}{k_B T_1}}{1 + \Gamma \cdot \frac{-E_a^i}{k_B T_2}}$$
(4)

where k_B is the Boltzmann constant, T_1 (300 K) is the initial temperature in Kelvin, T_2 is the final temperature of quenching, which in these calculations is 500 K, Γ is defined as the ratio of the attempt rate for thermal quenching (Γ_0) and the radiative decay rate of the 5d state (Γ_{ν}), ^{6,13} and E_a^i is the barrier for thermal ionization under the Dorenbos model.

The optimal values of *K*, *A*, *B*, *C*, *D*, and *E* (as defined in eq 3) were determined by performing a nonlinear least-squares minimization of the multivariable predicted TQ from eq 4 with the experimentally observed TQ of the 29 phosphors (see Table S1) and are tabulated in Table S2. The Ce³⁺- and Eu²⁺-

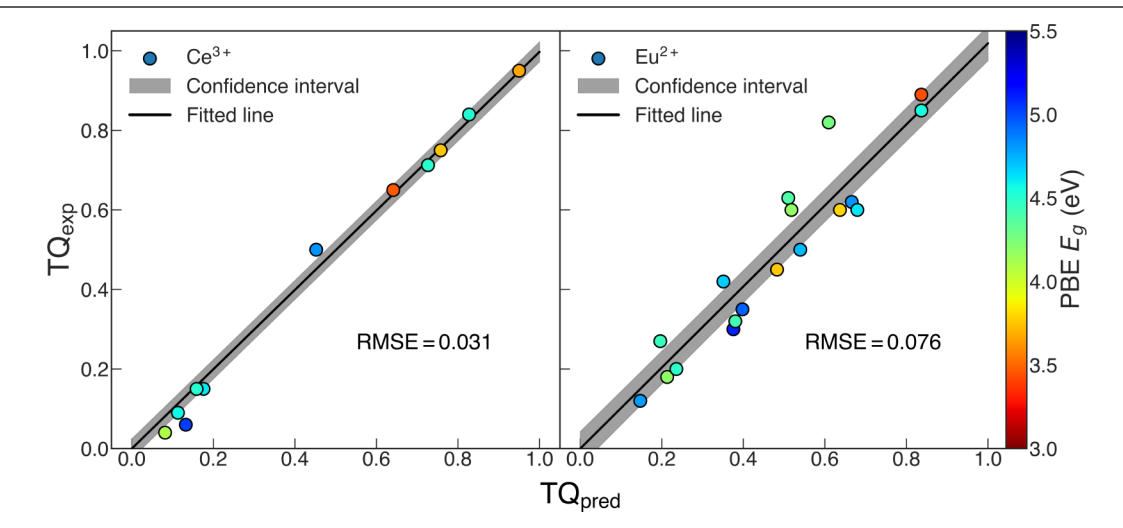


Figure 5. Unified TQ model prediction. Plot of TQ_{exp} against the predicted TQ_{pred} from the unified TQ model (eq 4) for Ce³⁺- (left) and Eu²⁺- (right) activated hosts. Here, RMSE is computed as follows: RMSE = $\sqrt{\frac{1}{N}\sum_{i=1}^{N}\left(\mathrm{TQ}_{\mathrm{exp}}^{i}-\mathrm{TQ}_{\mathrm{pred}}^{i}\right)^{2}}$.

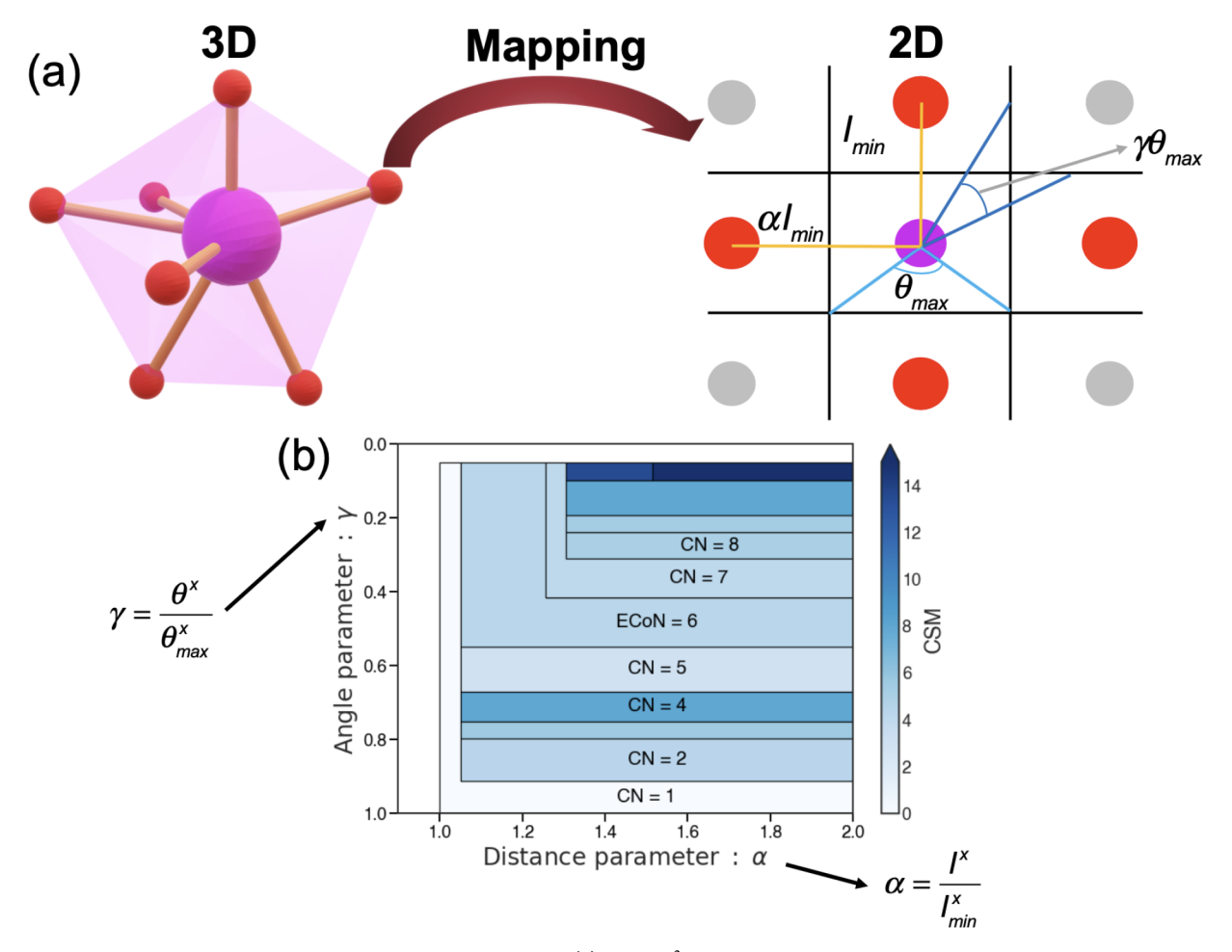


Figure 6. Intrinsic topological descriptor of the activator's rigidity. (a) The Eu^{2+} 3-dimensional local environment is mapped to a 2-dimensional representation by defining two parameters, the distance parameter α and the angle parameter γ . For each specific range of angle and distance parameters, a unique coordination number is defined. A graphical depiction of the 2-dimensional reduction is presented by (b) the Voronoi grid representation for Eu^{2+} in Sr_2SiO_4 . Each Voronoi grid representation is representative of a set of ligands denoted by its coordination number. The continuous symmetry measure is used to assess the degree of symmetry within different coordination numbers and was developed by Pinsky.³⁰

activated phosphors are expected to have different K, B, C, D, and E values because of their large difference in energy gap between the 4f ground state and the 5d excited state (6.2 and 4.2 eV for free Ce3+ and Eu2+ ions, respectively) and different ionic radii. ¹⁹ Most importantly, the band gap factors (A = 0.15and 0.19) for Ce³⁺ and Eu²⁺ are expected to be the same since both are computed using the same functional. Figure 5 plots the predicted TQ_{pred} using the optimized eq 4 against the experimental TQ_{exp}. The RMSEs for Ce³⁺ and Eu²⁺ are 3.1% and 7.6%, respectively, which are a significant improvement over those from the model using ΔAED alone. Further validation of our unified TQ model can be seen in the fact that the predicted E_a^i (Table S1) are in good agreement with experimental thermal ionization energies. For example, the predicted E_a^i of $Sr_2MgSi_2O_7:Eu^{2+}$, $SrSc_2O_4:Eu^{2+}$, Y₃Al₅O₁₂:Ce³⁺, Lu₃Al₅O₁₂:Ce³⁺, and K₃YSi₂O₇:Ce³⁺ are 0.87 eV, 0.71 eV, 0.88 eV, 0.87 eV, and 0.54 eV, respectively, and the corresponding experimental thermal ionization energies are 0.9 eV, 0.56 eV, 0.77 eV, 0.75 eV, and 0.48 eV, respectively. $^{13,20,23-25}$ Note that our predicted E_a^i for Y₃Al₅O₁₂:Ce³⁺ is higher than the predicted value for Lu₃Al₅O₁₂:Ce³⁺ as shown in the vacuum referenced binding energies diagram.²⁰

Previous measurements from Dorenbos have suggested that the redshift D (A^{x+} , H) (the sum of the centroid shift and the crystal splitting shift) of the 5d state of the Ce³⁺ activator is correlated to the one of the Eu²⁺ ion when inserted within the same host/site as follows:

$$D(Eu^{2+}, H) = 0.64 \cdot D(Ce^{3+}, H) - 0.233 \text{ eV} \pm 0.15$$

Equivalently, photoluminescence properties such as emission energy and activation energies of Ce^{3+} -doped phosphors can help assess the photoluminescence of Eu^{2+} when inserted within the same host/site. To further substantiate the validity of our fitted A, B, C, D, and E, we predict the E_a^i of $K_3YSi_2O_7$: Eu^{2+} from our fitted results of $K_3YSi_2O_7$: Ce^{3+} by utilizing Dorenbos's semiempirical relationship. The predicted E_a^i of Eu^{2+} doped in $K_3YSi_2O_7$ from the fitted parameters of Ce^{3+} -doped compounds are 0.65 eV, while the experimentally determined values are 0.63 eV, which are in excellent agreement.

The unified TQ equation (eq 4) can be understood intuitively by considering the competition between the crossover and thermal ionization mechanisms in Figure 1. The primary loss of emission with temperature increase will come from the mechanism with the lowest barrier E_a . When the band gap of the host is large, $E_a^i \gg E_a^{co}$, the crossover

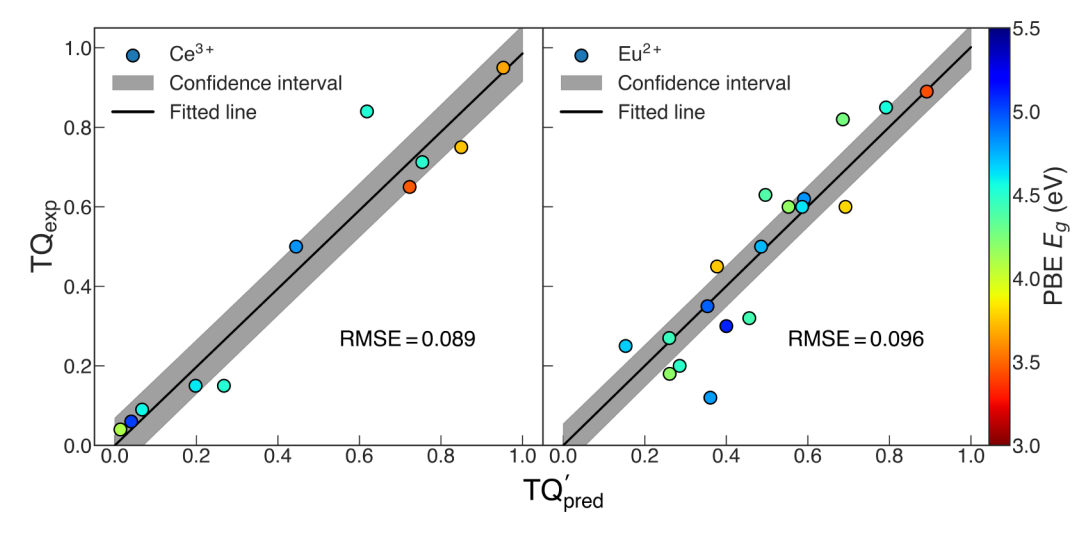


Figure 7. Plot of the predicted TQ'_{pred} against TQ_{exp} obtained from the modified TQ model utilizing the topological descriptor in eq 5 for Ce^{3+} (left) and Eu^{2+} (right) activated phosphors.

mechanism dominates. AAED then describes the depth of the potential energy surface and, hence, TQ. When the band gap of the host is sufficiently small, both mechanisms compete, and Δ AED, E_{g} , ε_{o} and ε_{cfs} are required to describe the TQ under a dual-barrier quenching model. Unlike the semiempirical thermal ionization relationship, the proposed unified TQ model allows for the first time to develop a universal comparison among all hosts' high temperature photoluminescence behavior via robust descriptors (Δ AED, E_{gr} ε_{o} and ε_{cfs}) obtained in a prehoc manner. Moreover, E_a^i derived from Dorenbos's semiempirical relationship is a function of $T_{1/2}$ (the temperature at which the intensity reaches half of the initial intensity), where the latter varies for every host. Consequently, all previously obtained E_a^i values mentioned in the literature reflect a thermal quenching occurring across different temperatures ranges, and hence cross-comparisons of E_a^i were impossible and impractical until now. Finally, while the proposed dual-barrier thermal quenching offers a comprehensive overview of the TQ mechanism, its applicability cannot directly be extended to phosphors with multiple luminescent centers, as the AED and electronic properties are expected to differ from the pristine structure. Additionally, phosphors known to have photoluminescence compensation mechanisms driven by the formation of thermally activated defect levels are also not within the scope of the dual-barrier quenching model;²⁶⁻²⁸ however, with enough data, an additive model accounting for the electronic contributions of defects can potentially be derived.

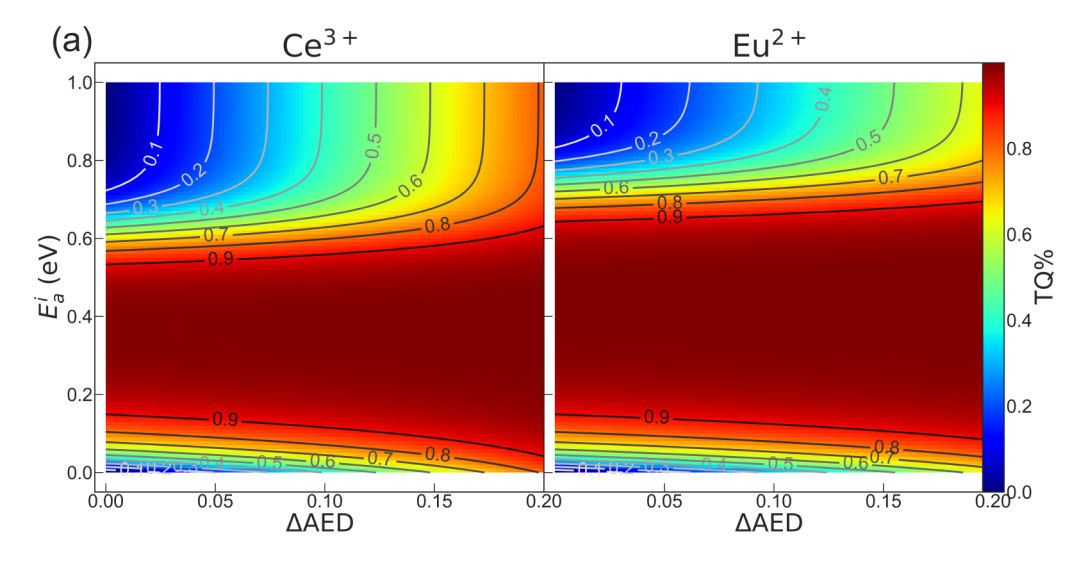
Intrinsic Topological Descriptor of the Activator's Stability. Finally, we demonstrate how a modified version of the unified TQ model can be used to computationally screen for low TQ phosphors. While E_g^{DFT} , ε_o and ε_{cfs} can be obtained using relatively inexpensive ground-state DFT computations, Δ AED requires expensive AIMD simulations for activated phosphors, where relatively large supercells of the host crystal are required to simulate the experimental low activator concentration. It is, therefore, desirable to establish an alternative descriptor for local environment stability. The AEDs at 300 and 500 K reveal that activators are susceptible to endure local polyhedron changes due to mutual oscillations of the centroid/activator and ligands/oxygen in the first shell. The computed mean-square displacements (MSD) of the

activator and oxygen ligands increase from 300 and 500 K, suggesting that the overall occupied 3-dimensional space by the activator and ligands increases with temperature. For example, the MSD behavior of Ce³⁺ and oxygen ligands in the first shell in the Ca₃Sc₂Si₃O₁₂ host is shown in Figure S6a; a definite increase in the MSD for both Ce³⁺ and oxygen ligands with respect to temperature is observed. Despite large atomic displacements in the Ca₃Sc₂Si₃O₁₂ host, the periodic-like oscillations of both Ce3+ and oxygen ligands result in a low ΔAED. Conversely, the MSD behavior of Ce³⁺ and oxygen ligands in the Ba₃Y₂B₆O₁₅ host (Figure S6b) shows a quasirandom oscillation resulting in a larger ΔAED . The same observations can be made for SrMgAl₁₀O₁₇:Eu²⁺ and Ba₂SiO₄:Eu²⁺ (Figure S6c,d). Consequently, smaller ΔAED values are suspected to be correlated to large 3-dimensional spaces around Hoppe's²⁹ effective activator local environment.

Two-dimensional projections (Figure 6a) of all Ce³⁺/Eu²⁺ local environments in the 29 hosts were constructed via a Voronoi tessellation-based algorithm. 12 Figure 6b shows a topological sensitivity analysis of the local activator environment of Eu2+ in Sr2SiO4 (similar plots for all of the 29 phosphors are provided in the Supporting InformationFigures S6 and S7). By varying the distance (α) and angle (γ) parameters, the algorithm yields different coordination environments due to changes in the bond weights of the surrounding ligands as shown in Figure 6b (refer to eq S2 in the Supporting Information). The coordination environment formed by the highest weight ligands determines the main activator local environment, which in Sr₂SiO₄:Eu²⁺ is an effective coordination number (ECoN) of 6. Our hypothesis is that the larger the normalized area (Υ) occupied by the main activator local environment, the less sensitive the activator local environment is to variations in bond distances and angles. In other words, the higher the Υ , the lower the Δ AED and the smaller the expected TQ. Therefore, substituting \triangle AED with 1 $-\Upsilon$ in eq 4, we obtain the following alternative model:

$$TQ = 1 - K' \cdot (1 - Y) \frac{1 + \Gamma' \cdot \frac{-E_a'}{k_B T_1}}{1 + \Gamma' \cdot \frac{-E_a'}{k_B T_2}}$$
(5)

where A, B, C, D, and E for the E_a^i expression in eq 3 are kept as the optimized values from the nonlinear least-squares



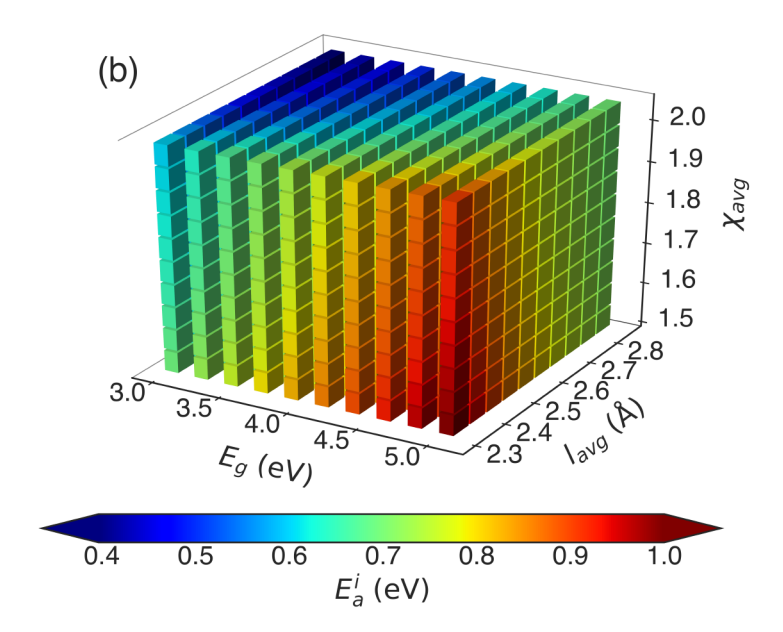


Figure 8. Phosphor design maps. (a) Plots of the predicted TQ as a functional of ΔAED and E_a^i . (b) Plot of the predicted thermal ionization barrier for a cubic geometry.

optimization of eq 4, while K' is refitted. The optimized values of K' are 0.27 and 0.77 for Ce^{3+} and $Eu^{\overline{2}+}$, respectively (included in Table S2). Moreover, the computed E_a^i as defined in eq 4 is based on the rate of change of Δ AED across all of the 29 compounds, and Δ AED does not scale linearly with respect to Y. Therefore, to compensate for the different rates of \triangle AED and Υ , the pre-exponential factor is redefined as $\Gamma' = \beta \Gamma$. The optimized values of β for Ce³⁺ and Eu²⁺ were 2.75 and 0.86, respectively (shown in Table S2). Figure 7 plots TQ_{exp} against TQ'_{pred} as defined by eq 5. The RMSEs of TQ'_{pred} for Ce³⁺ and Eu²⁺ are 8.9% and 9.6%, respectively. While this value of RMSE is somewhat higher than the RMSE using eq 4, the RMSE using eq 5 is already sufficiently low for Ce³⁺/Eu²⁺activated hosts to be used for rapid screening for discovery of low TQ phosphors. The difference in performance between using $(1 - \Upsilon)$ and Δ AED, especially for Ce³⁺-activated hosts, can be attributed to two factors. First, some of the considered compounds are known to have multiple symmetrically distinct doping sites, i.e., $Ba_3Y_2B_6O_{15}:Ce^{3+}$ and $Ba_9Y_2(SiO_4)_6:Ce^{3+}$, while the Voronoi area was computed using only the most energetically stable site. Second, $(1-\Upsilon)$ is a pure topological descriptor with no consideration of differences in chemical bonding, whereas ΔAED captures subtle relationships between bond distances, bond angle,s and bond strength in the distribution of activator environments. Nevertheless, the ability to quickly obtain Υ values without computationally expensive AIMD calculations makes this approach ideal for materials screening.

Phosphor Design Map. Using the models developed above, we have constructed phosphor design maps for the Ce^{3+} and Eu^{2+} phosphors as shown in Figure 8. It can be seen that to achieve low TQs < 20%, small $\Delta AEDs$ of less than 0.05 are needed as well as high thermal ionization barriers $E_a^i > 0.75$ and 0.82 eV for Ce^{3+} and Eu^{2+} activators, respectively. Based on eq 2, E_a^i is a function of E_g , ε_o and ε_{gfs} . ε_c is a function of average bond length l_{avg} and the average electronegativity of

the cation χ_{avg} , while ε_{cfs} depends on the polyhedron shape (CN and geometry) and size (l_{avg}) . Figure 8b shows a 4-dimensional plot of E_a^i as a function of E_g , l_{avg} , and χ_{avg} for a cubic environment (similar maps for the octahedral environment are given in the Supporting Information Figure S9). At sufficiently large $E_g > 4$ eV, E_a^i above the necessary thresholds for low TQ can be achieved for a wide range of l_{avg} and χ_{avg} . This suggests that meeting the requirement of low ΔAED would be the dominant criterion for large band gap phosphors, i.e., short wavelength emission. At low $E_g < 4$ eV, i.e., longwavelength phosphors, meeting the E_a^i threshold for low TQ based on thermal ionization requires careful selection of compositions to tune l_{avg} and χ_{avg} .

CONCLUSION

In summary, we have developed a unified dual-barrier TQ model by integrating the two prevailing theories—the crossover and thermal ionization models-for thermal quenching in Ce3+- and Eu2+-activated phosphors. More critically, we have developed computational approaches to probe thermal quenching in phosphors using this unified TQ model. We establish that the local activator environment stability, as measured by the change in activator environment distribution with temperature in AIMD simulations, Δ AED, is the relevant descriptor for TQ under the crossover mechanism. The computed host band gap (E_{σ}) , the centroid shift (ε_{c}) , and the approximated crystal-field splitting (ε_{cfs}) are descriptors for TQ under the thermal ionization mechanism. This unified dual-barrier thermal quenching model combining ΔAED , E_{g} , ε_{o} and ε_{cf} , predicts the experimentally observed TQ in 29 Ce^{3‡}and Eu²⁺-activated phosphors to within an RMSE of 3.1% and 7.6%, respectively. We have also developed an alternative topological descriptor for local environment stability based on Voronoi tessellation that allows for rapid TQ screening of phosphors without expensive AIMD simulations. It should be noted that while the focus of this work is on oxide phosphors, the approach can be readily extended to other chemistries such as nitrides, though the fitted model parameters would be different. This would be the subject of future work. This work provides crucial insights into the TQ mechanisms in phosphors and an efficient and reliable path to the discovery of new phosphors with low TQ for next-generation, high power solidstate lighting.

■ METHODS

Density Functional Theory (DFT) Calculations. All DFT calculations were performed using the Vienna ab initio simulation package (VASP) within the projector-augmented wave method. 33,3 The exchange-correlation interaction was described using the Perdew-Burke-Ernzerhof (PBE)³⁴ generalized gradient approximation (GGA) functional with the Hubbard U extension. In general, the parameters used are similar to those used in the Materials Project,³ with a plane wave energy cutoff of 520 eV and a k-point density at least of 100 per $Å^{-3}$. A U value of 2.5 eV was used for the 4f orbitals in Eu and Ce following previous works. 32,36 All structures were fully relaxed with energies, and forces converged to within 10⁻⁵ eV and 0.01 eV Å⁻¹, respectively. To construct the Ce³⁺/Eu²⁺-activated phosphors, Ce3+/Eu2+ was doped into all compatible symmetrically distinct sites in supercells of the host crystal with lattice parameters of at least 10 Å in each direction. The lowest energy Ce3+/Eu2+-doped structure was then used for subsequent analysis and AIMD simulations. All crystal structure and data analyses were carried out using the Python Materials Genomics (pymatgen) package.3

Ab initio molecular dynamics (AIMD) simulations were carried out on the supercell models of Ce^{3+}/Eu^{2+} -activated phosphors in the NVT ensemble at 300 and 500 K with a Nose-Hoover thermostat. The simulation cell was fixed at the final 0 K relaxed cell parameters for each phosphor. For reasons of computational efficiency, the AIMD simulations were nonspin-polarized, and a minimal Γ-centered 1 × 1 × 1 k-point mesh and a time step of 2 fs were adopted. Given that the main output extracted from the AIMD simulations is the local environment fluctuations, we expect this approximation to be reasonable.

ASSOCIATED CONTENT

Supporting Information

The Supporting Information is available free of charge at https://pubs.acs.org/doi/10.1021/acs.chemmater.0c02231.

Derivation of the unified thermal quenching model, structural and thermal quenching properties for 29 oxide phosphors, optimized coefficients from the nonlinear least-squared minimization of the unified TQ model for Ce^{3+} - and Eu^{2+} -activated hosts, activator environment distribution for Ce^{3+} -activated hosts at 300 and 500 K, activator environment distribution for Eu^{2+} -activated hosts at 300 and 500 K, experimentally measured thermal quenching (TQ_{exp}) against the DFT-calculated Debye temperature (Θ_D), mean-square displacements (MSD) against time (fs) of Ce^{3+}/Eu^{2+} and oxygen ligands ($O_{ligands}$), Voronoi grid representation of the Ce^{3+} local environment of all the Ce^{3+} -activated hosts in Table S1, Voronoi grid representation of the Eu^{2+} local environment of all the Eu^{2+} -activated hosts in Table S1, and plot of the predicted thermal ionization barrier for an activator with an octahedron geometry (PDF)

AUTHOR INFORMATION

Corresponding Author

Shyue Ping Ong — Department of NanoEngineering, University of California San Diego, La Jolla, California 92093-0448, United States; ⊚ orcid.org/0000-0001-5726-2587; Email: ongsp@eng.ucsd.edu

Authors

Mahdi Amachraa — Materials Science and Engineering Program, University of California San Diego, La Jolla, California 92093-0448, United States; ⊚ orcid.org/0000-0003-3001-3630

Zhenbin Wang – Materials Science and Engineering Program, University of California San Diego, La Jolla, California 92093-0448, United States

Chi Chen – Department of NanoEngineering, University of California San Diego, La Jolla, California 92093-0448, United States

Shruti Hariyani — Department of Chemistry, University of Houston, College of Natural Sciences and Mathematics, Houston, Texas 77204-5008, United States

Hanmei Tang — Materials Science and Engineering Program, University of California San Diego, La Jolla, California 92093-0448, United States; ⊚ orcid.org/0000-0003-2659-7768

Jakoah Brgoch — Department of Chemistry, University of Houston, College of Natural Sciences and Mathematics, Houston, Texas 77204-5008, United States; ⊙ orcid.org/0000-0002-1406-1352

Complete contact information is available at: https://pubs.acs.org/10.1021/acs.chemmater.0c02231

Author Contributions

§(M.A. and Z.W.) These authors contributed equally

Notes

The authors declare no competing financial interest.

ACKNOWLEDGMENTS

This work was primarily supported by the National Science Foundation, Ceramics Program, under grant No. 1911372. S.H. and J.B. also acknowledge funding from the National Science Foundation under Grant No. 1911311. The computational resources were provided by the Extreme Science and Engineering Discovering Environment (XSEDE) supported by the National Science Foundation under Grant No. ACI-1548562, the Triton Super Computer Center (TSCC) at the University of California, San Diego, and the National Energy Research Scientific Computing Center (NERSC).

REFERENCES

- (1) Penning, J.; Stober, K.; Taylor, V.; Yamada, M. Energy Savings Forecast of Solid-State Lighting in General Illumination Applications; U.S. Department of Energy: 2016; https://www.osti.gov/servlets/purl/1374119 (accessed April 10, 2020).
- (2) Brinkley, S. E.; Pfaff, N.; Denault, K. A.; Zhang, Z.; Hintzen, H. T.; Seshadri, R.; Nakamura, S.; DenBaars, S. P. Robust thermal performance of Sr₂Si₃N₈:Eu²⁺: An efficient red emitting phosphor for light emitting diode based white lighting. *Appl. Phys. Lett.* **2011**, *99*, 241106.
- (3) Poncé, S.; Jia, Y.; Giantomassi, M.; Mikami, M.; Gonze, X. Understanding Thermal Quenching of Photoluminescence in Oxynitride Phosphors from First Principles. *J. Phys. Chem. C* **2016**, *120*, 4040–4047.
- (4) Denault, K. A.; Brgoch, J.; Kloß, S. D.; Gaultois, M. W.; Siewenie, J.; Page, K.; Seshadri, R. Average and Local Structure, Debye Temperature, and Structural Rigidity in Some Oxide Compounds Related to Phosphor Hosts. *ACS Appl. Mater. Interfaces* **2015**, *7*, 7264–7272.
- (5) Zhuo, Y.; Mansouri Tehrani, A.; Oliynyk, A. O.; Duke, A. C.; Brgoch, J. Identifying an efficient, thermally robust inorganic phosphor host via machine learning. *Nat. Commun.* **2018**, *9*, 4377.
- (6) Dorenbos, P. Thermal quenching of Eu²⁺ 5d-4f luminescence in inorganic compounds. *J. Phys.: Condens. Matter* **2005**, *17*, 8103–8111.
- (7) Blasse, G.; Bril, A. Characteristic luminescence. *Philos. Technol. Rev.* 1970, 31, 304–314.
- (8) Blasse, G.; Grabmaier, B. C. Luminescent Materials; Springer Berlin Heidelberg: Berlin, Heidelberg, 1994; DOI: 10.1007/978-3-642-79017-1.
- (9) Ha, J.; Wang, Z.; Novitskaya, E.; Hirata, G. A.; Graeve, O. A.; Ong, S. P.; McKittrick, J. An integrated first principles and experimental investigation of the relationship between structural rigidity and quantum efficiency in phosphors for solid state lighting. *J. Lumin.* **2016**, *179*, 297–305.
- (10) Duke, A. C.; Finley, E.; Hermus, M.; Brgoch, J. Yellow-green luminescence and extreme thermal quenching in the $Sr_6M_2Al_4O_{15}$: Eu^{2+} (M = Y, Lu, Sc) phosphor series. *Solid State Sci.* **2016**, *60*, 108–113.
- (11) Nemitz, W.; Fulmek, P.; Nicolics, J.; Reil, F.; Wenzl, F. P. On the determination of the temperature distribution within the color conversion elements of phosphor converted LEDs. Sci. Rep. 2017, 7, 9964
- (12) Waroquiers, D.; Gonze, X.; Rignanese, G. M.; Welker-Nieuwoudt, C.; Rosowski, F.; Göbel, M.; Schenk, S.; Degelmann, P.; André, R.; Glaum, R.; Hautier, G. Statistical analysis of coordination environments in Oxides. *Chem. Mater.* **2017**, *29*, 8346–8360.
- (13) Ueda, J.; Dorenbos, P.; Bos, A. J. J.; Meijerink, A.; Tanabe, S. Insight into the Thermal Quenching Mechanism for $Y_3Al_5O_{12}$: Ce^{3+}

- through Thermoluminescence Excitation Spectroscopy. *J. Phys. Chem.* C 2015, 119, 25003–25008.
- (14) Li, K.; Liang, S.; Lian, H.; Shang, M.; Xing, B.; Lin, J. Ce³⁺ and Tb³⁺-doped lutetium-containing silicate phosphors: Synthesis, structure refinement and photoluminescence properties. *J. Mater. Chem. C* **2016**, *4*, 3443–3453.
- (15) Hermus, M.; Phan, P.-C.; Brgoch, J. Ab Initio Structure Determination and Photoluminescent Properties of an Efficient, Thermally Stable Blue Phosphor, Ba₂Y₅B₅O₁₇:Ce³⁺. *Chem. Mater.* **2016**, 28, 1121–1127.
- (16) Wang, Z.; Ha, J.; Kim, Y. H.; Im, W. B.; McKittrick, J.; Ong, S. P. Mining Unexplored Chemistries for Phosphors for High-Color-Quality White-Light-Emitting Diodes. *Joule* **2018**, *2*, 914–926.
- (17) Lu, F.-C.; Bai, L.-J.; Dang, W.; Yang, Z.-P.; Lin, P. Structure and Photoluminescence of Eu²⁺ Doped Sr₂Al₂SiO₇ Cyan-Green Emitting Phosphors. ECS J. Solid State Sci. Technol. **2015**, 4, R27–R30.
- (18) Komuro, N.; Mikami, M.; Shimomura, Y.; Bithell, E. G.; Cheetham, A. K. Synthesis, structure and optical properties of europium doped calcium barium phosphate-a novel phosphor for solid-state lighting. *J. Mater. Chem. C* **2014**, *2*, 6084–6084.
- (19) Dorenbos, P. Relation between Eu²⁺ and Ce³⁺ f d-transition energies in inorganic compounds. *J. Phys.: Condens. Matter* **2003**, *15*, 4797–4807.
- (20) Dorenbos, P. A Review on How Lanthanide Impurity Levels Change with Chemistry and Structure of Inorganic Compounds. *ECS J. Solid State Sci. Technol.* **2013**, 2, R3001–R3011.
- (21) Görller-Walrand, C.; Binnemans, K. Handbook on the Physics and Chemistry of Rare Earths; Elsevier: 1996; Vol. 23, pp 121–283.
- (22) Perdew, J. P. Density functional theory and the band gap problem. *Int. J. Quantum Chem.* **1985**, 28, 497–523.
- (23) Hölsä, J.; Kirm, M.; Laamanen, T.; Lastusaari, M.; Niittykoski, J.; Novák, P. Electronic structure of the Sr₂MgSi₂O₇:Eu²⁺ persistent luminescence material. *J. Lumin.* **2009**, *129*, 1560–1563.
- (24) Müller, M.; Volhard, M. F.; Jüstel, T. Photoluminescence and afterglow of deep red emitting SrSc₂O₄:Eu²⁺. RSC Adv. **2016**, 6, 8483–8488.
- (25) Qiao, J.; Amachraa, M.; Molokeev, M.; Chuang, Y. C.; Ong, S. P.; Zhang, Q.; Xia, Z. Engineering of K₃YSi₂O₇ to Tune Photoluminescence with Selected Activators and Site Occupancy. *Chem. Mater.* **2019**, *31*, 7770–7778.
- (26) Kim, Y. H.; Arunkumar, P.; Kim, B. Y.; Unithrattil, S.; Kim, E.; Moon, S.-H.; Hyun, J. Y.; Kim, K. H.; Lee, D.; Lee, J.-S.; Im, W. B. A zero-thermal-quenching phosphor. *Nat. Mater.* **2017**, *16*, 543–550.
- (27) Cheng, C.; Ning, L.; Ke, X.; Molokeev, M. S.; Wang, Z.; Zhou, G.; Chuang, Y. C.; Xia, Z. Designing High-Performance LED Phosphors by Controlling the Phase Stability via a Heterovalent Substitution Strategy. *Adv. Opt. Mater.* **2020**, *8*, 1901608.
- (28) Zhao, M.; Xia, Z.; Huang, X.; Ning, L.; Gautier, R.; Molokeev, M. S.; Zhou, Y.; Chuang, Y. C.; Zhang, Q.; Liu, Q.; Poeppelmeier, K. R. Li substituent tuning of LED phosphors with enhanced efficiency, tunable photoluminescence, and improved thermal stability. *Science Advances* **2019**, *5*, eaav0363.
- (29) Hoppe, R. The Coordination Number an "Inorganic Chameleon. *Angew. Chem., Int. Ed. Engl.* **1970**, *9*, 25–34.
- (30) Pinsky, M.; Avnir, D. Continuous Symmetry Measures. 5. The Classical Polyhedra. *Inorg. Chem.* **1998**, *37*, 5575–5582.
- (31) Brgoch, J.; Borg, C. K. H.; Denault, K. A.; Mikhailovsky, A.; Denbaars, S. P.; Seshadri, R. An efficient, thermally stable ceriumbased silicate phosphor for solid state white lighting. *Inorg. Chem.* **2013**, *52*, 8010–8016.
- (32) Kresse, G.; Furthmüller, J. Efficient iterative schemes for ab initio total-energy calculations using a plane-wave basis set. *Phys. Rev. B: Condens. Matter Mater. Phys.* **1996**, *54*, 11169–11186.
- (33) Blöchl, P. E. Projector augmented-wave method. *Phys. Rev. B: Condens. Matter Mater. Phys.* **1994**, *50*, 17953–17979.
- (34) Perdew, J. P.; Burke, K.; Ernzerhof, M. Generalized Gradient Approximation Made Simple. *Phys. Rev. Lett.* **1996**, *77*, 3865–3868.
- (35) Ong, S. P.; Cholia, S.; Jain, A.; Brafman, M.; Gunter, D.; Ceder, G.; Persson, K. A. The Materials Application Programming Interface

- (API): A simple, flexible and efficient API for materials data based on REpresentational State Transfer (REST) principles. *Comput. Mater. Sci.* **2015**, 97, 209–215.
- (36) Chaudhry, A.; Boutchko, R.; Chourou, S.; Zhang, G.; Grønbech-Jensen, N.; Canning, A. First-principles study of luminescence in Eu²⁺-doped inorganic scintillators. *Phys. Rev. B: Condens. Matter Mater. Phys.* **2014**, 89, 155105.
- (37) Ong, S. P.; Richards, W. D.; Jain, A.; Hautier, G.; Kocher, M.; Cholia, S.; Gunter, D.; Chevrier, V. L.; Persson, K. A.; Ceder, G. Python Materials Genomics (pymatgen): A robust, open-source python library for materials analysis. *Comput. Mater. Sci.* **2013**, *68*, 314–319.
- (38) Hoover, W. G. Canonical dynamics: Equilibrium phase-space distributions. *Phys. Rev. A: At., Mol., Opt. Phys.* **1985**, 31, 1695–1697.